ACS OMEGA

Open Access

http://pubs.acs.org/journal/acsodf

Article

A Preliminary Study of Spherical Surface-Modified Carbon Materials for Potential Application in La^{3+} (Ac^{3+}) and Bi^{3+} Separation

Hongshan Zhu, Stephan Heinitz, Koen Binnemans, Steven Mullens, and Thomas Cardinaels*

Cite This: *ACS Omega* 2024, 9, 51009−51021

Read Online

ACCESS | Metrics & More | Article Recommendations | Supporting Information

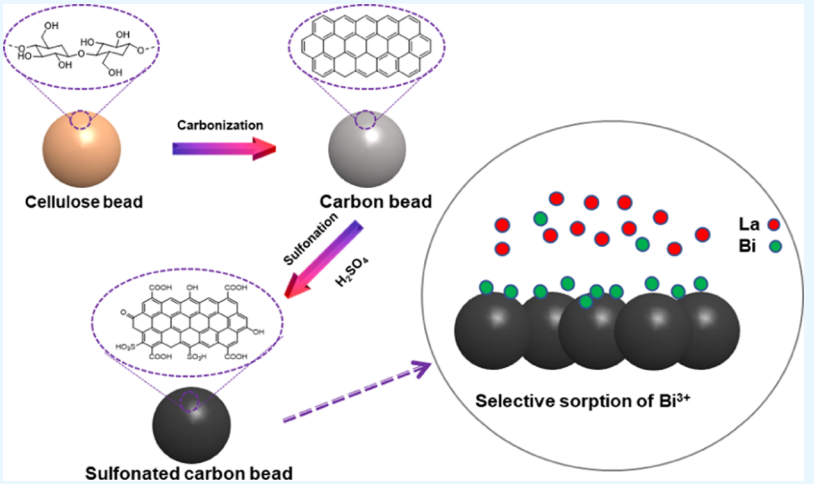

ABSTRACT: Separation of high-activity ^{213}Bi from ^{225}Ac for targeted alpha therapy is challenging due to the instability of existing sorbents. Surface-modified carbon materials have shown promise for use in inverse $^{225}Ac/^{213}Bi$ generators. However, previously reported materials with irregular shapes may limit their applications in column separations. In contrast, spherical particles are expected to be more suitable for column chromatography compared to irregular powders as they can ensure uniform flow patterns, lower pressure drop, and effective packing. To address this limitation, a method was developed for the synthesis of spherical carbon beads via the carbonization of cellulose beads. Subsequently, surface modification on the spherical carbon beads was performed via sulfonation or oxidation of the carbon beads. Batch sorption experiments were conducted to assess their selective sorption toward Bi^{3+} over La^{3+} (as a surrogate of Ac^{3+}) by varying the concentrations of HNO_3 and $NaNO_3$. It was found that the selective sorption of Bi^{3+} onto spherical surface-modified carbon beads could be achieved by adjusting the concentrations of HNO_3 and $NaNO_3$. Furthermore, the sorption capacity of Bi^{3+} decreased as the concentration of HCl increased due to the formation of bichloride complexes and the H^+ competition. This implies that Bi^{3+} can be effectively eluted from the spherical surface-modified carbon beads when using HCl as the eluate. Consequently, spherical surface-modified carbon beads show potential as alternative adsorbents for inverse $^{225}Ac/^{213}Bi$ generators.

1. INTRODUCTION

Targeted alpha therapy (TAT) has gained significant attention as a rapidly advancing field in cancer treatment.[1−4] Bismuth−213 (^{213}Bi) stands out as an intriguing radioisotope owing to its unique decay pathway, energy emissions from its daughter nuclide polonium-213 (^{213}Po), optimal range (40−100 μm), short half-life (45.6 min), and favorable chemical properties.[5−7] The relatively long-lived parent nuclide ^{225}Ac has been utilized as the primary source for producing ^{213}Bi, which can be separated using radionuclide generators.[8,9] These generators must deliver consistently high yields and exceptional ^{213}Bi purity to fulfill the increasing demand in clinical studies. Various materials, such as organic resins, silica-based materials, and zirconia-based materials, have been tested for $^{225}Ac/^{213}Bi$ generators.[10−15] However, these sorbent materials fall short of meeting the requirements for producing high activity of ^{213}Bi due to limitations regarding their shelf life, radiation stability, chemical stability, and ^{213}Bi yield.[8,16−21]

An inverse generator is an effective choice in terms of reducing the radiolytic damage to the sorbents by minimizing the contact

Received: June 11, 2024
Revised: September 12, 2024
Accepted: November 27, 2024
Published: December 16, 2024

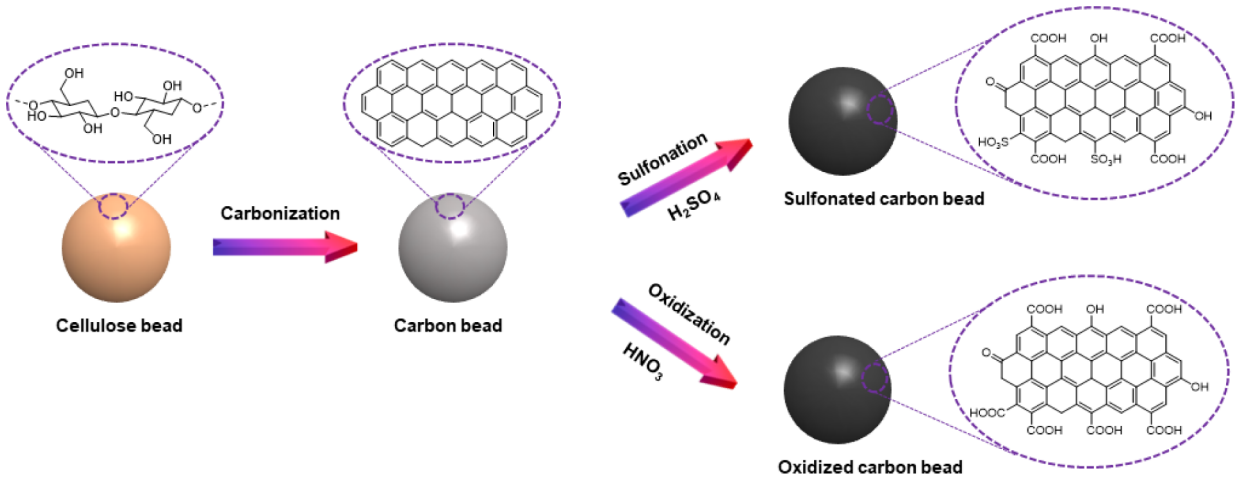

Figure 1. Pathways of formation of spherical surface-modified carbon beads.

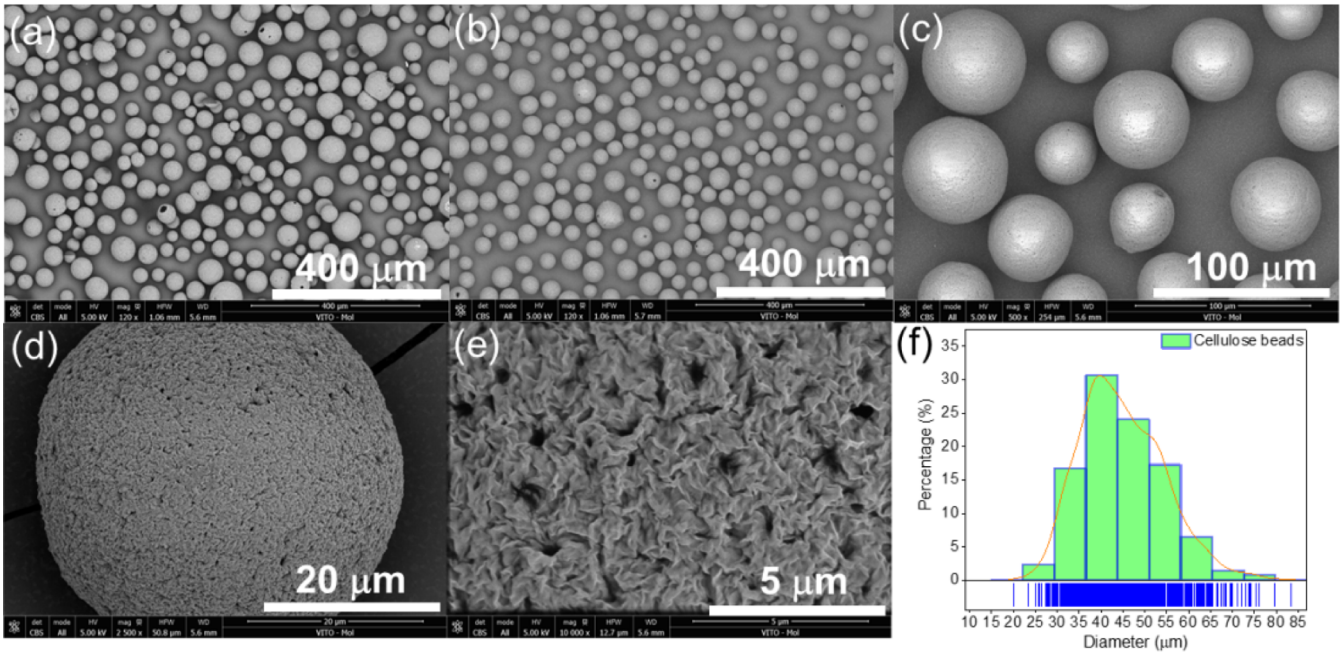

Figure 2. SEM images (a−e) and particle size distribution (f) of dried cellulose beads.

time.[11,13,22] Instead of sorbing the parent isotope ^{225}Ac onto the stationary phase, it is kept in the solution to allow for the ingrowth of ^{213}Bi, thereby significantly reducing radiation exposure to sorbents. As the ^{225}Ac/^{213}Bi solution passes through the inverse generator, ^{213}Bi can be selectively retained on the sorbent and subsequently eluted from the column.[17] McAlister et al. conducted an investigation into the efficacy of UTEVA resin for inverse ^{225}Ac/^{213}Bi generators.[11] However, UTEVA resin proved susceptible to radiation damage, leading to a rapid decline in its sorption capacity for ^{213}Bi as the absorbed radiation doses increased.[8] An inorganic material known as Termoxide-39 (T-39, composed of TiO_2 and Y_2O_3) exhibited high radiation stability and was tested for use in an inverse ^{225}Ac/^{213}Bi generator.[13] T-39 displayed promising prospects for application in inverse automatic generator systems.[13,23] However, the potential leaching of Zr or Y ions from T-39 when exposed to acidic solutions (e.g., 1 mol L^{-1} HCl) might lead to a reduction in ^{213}Bi yield and compromised chemical purity.[14] Therefore, the exploration of alternative sorbents with high radiolytic and chemical stabilities is the preferred approach for use in inverse generators.

Inverse generators have generated interest in utilizing carbon materials with high chemical and physical stability.[17,18,24] The surface of these materials can be tailored through grafting or impregnation methods to improve their active sorption sites. Surface-modified carbon materials with oxygen-containing groups exhibit selective sorption performance for Bi^{3+} by adjusting the pH condition and salt concentration.[17,18] In column chromatography, sulfonated carbon materials have shown promise in providing a high ^{213}Bi yield with acceptable ^{225}Ac impurities (e.g., < 0.1%). To further purify the ^{213}Bi eluate, a second column containing AG MP-50 resin is expected to be utilized, meeting the requirements for subsequent radiolabeling steps.[17] However, the reported surface-modified carbon materials have irregular particle shapes. In terms of column chromatography, the morphology of the sorbents plays a crucial role in column performance. Unlike granular particles, spherical particles ensure uniform flow patterns, lower pressure drop, and

https://doi.org/10.1021/acsomega.4c05457
ACS Omega 2024, 9, 51009−51021

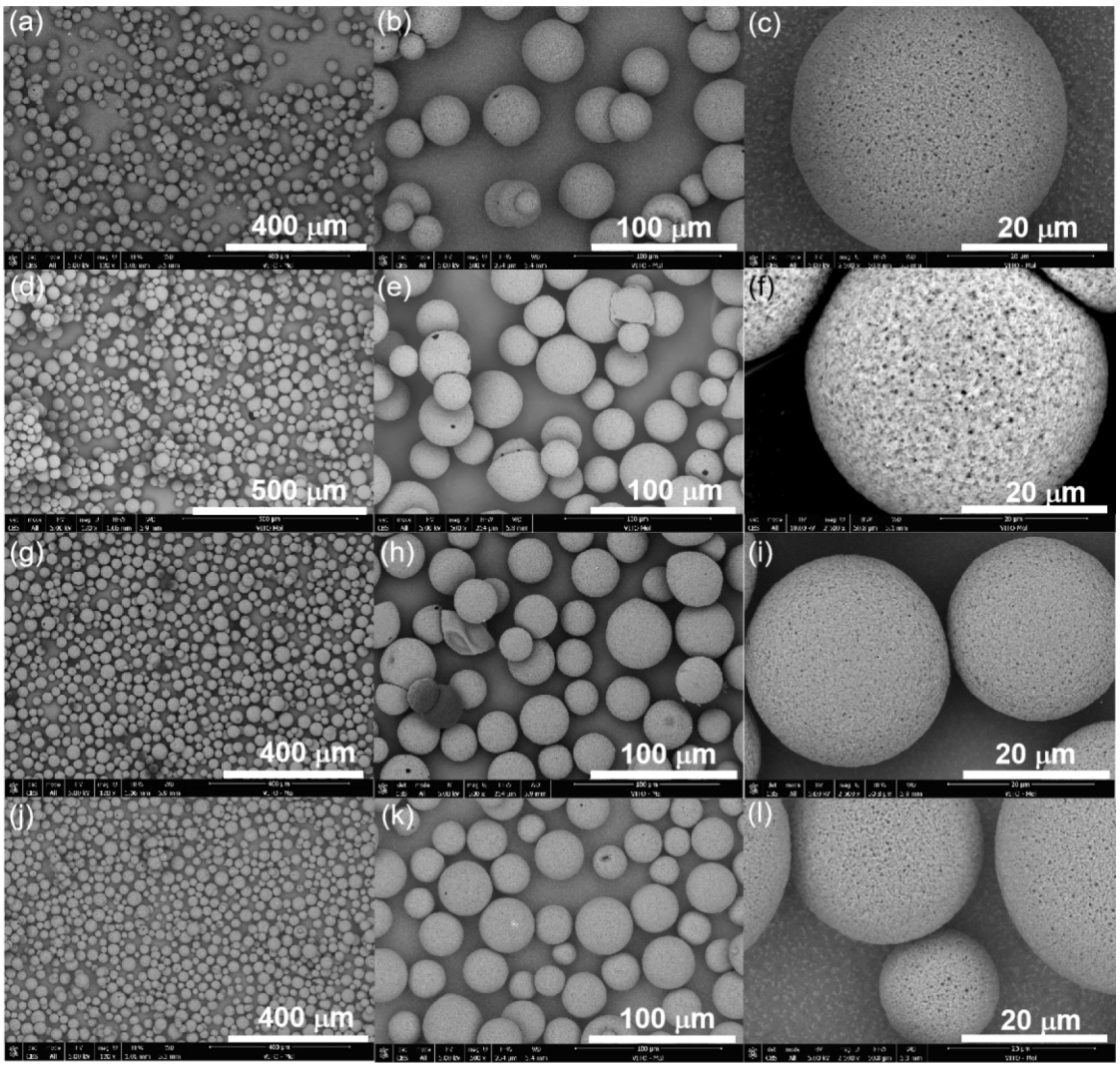

Figure 3. SEM images of CB-400 (a–c), CB-450 (d–f), CB-500 (g–i), and CB-800 (j–l).

effective packing.[25,26] Therefore, the synthesis of spherical carbon materials is vital to optimizing their performance in column chromatography.

The synthesis of spherical carbon materials has conventionally involved the carbonization of spherical polymeric precursors, spherical lignocellulosic precursors, and other precursors.[27,28] Among these, spherical cellulose beads are promising precursors for the formation of spherical carbon beads due to their abundance and renewable nature.[29−31] Various techniques such as dropping, jet cutting, spinning drop atomization, and spraying dispersion have been utilized to design spherical cellulose beads.[27] However, synthesizing spherical carbon beads with particle sizes ranging from 20 to 300 μm remains a challenge. Therefore, prior to optimizing particle sizes, it is necessary to conduct a preliminary investigation on the potential use of spherical carbon beads or their derivatives for ^{225}Ac and ^{213}Bi applications. In the preliminary study, commercially available cellulose beads were selected. Several sorbent characteristics, such as surface functional groups, surface areas, pore structure, and carbon structures, can influence the separation performance of ^{225}Ac and ^{213}Bi.[17,18] Initially, carbon materials may have insufficient amounts of functional groups on their surface due to the carbonization step often performed during their synthesis, which is accompanied by the vaporization of volatile compounds containing elements such as N, O, S, and P. Building upon previous work, surface modifications, specifically sulfonation and oxidation treatments, would be suitable strategies for directly grafting oxygen-containing groups onto carbon structures to enhance the sorption capacity for $^{213}Bi^{3+}$.[17,18]

In this study, spherical surface-modified carbon materials were prepared through the pyrolysis of cellulose beads, followed by a sulfonation/oxidation process, as depicted in Figure 1. Concentrated sulfuric acid and nitric acid were used as the reagents for the sulfonation and oxidization process, respectively. The characterization of morphology characteristics, elemental compositions, and functional groups was examined. Batch sorption experiments were performed to optimize the separation process, investigating various factors, such as HNO_3, $NaNO_3$, and HCl concentrations. The results of this work provide compelling evidence for the utilization of spherical surface-modified carbon beads in inverse generators. Hence, the synthesis of spherical carbon beads with different particle sizes holds significant importance and necessitates further exploration in future studies.

2. EXPERIMENTAL SECTION

2.1. Chemicals and Materials. Cellufine GH-25 with a matrix of cross-linked cellulose was purchased from JNC

https://doi.org/10.1021/acsomega.4c05457
ACS Omega 2024, 9, 51009−51021

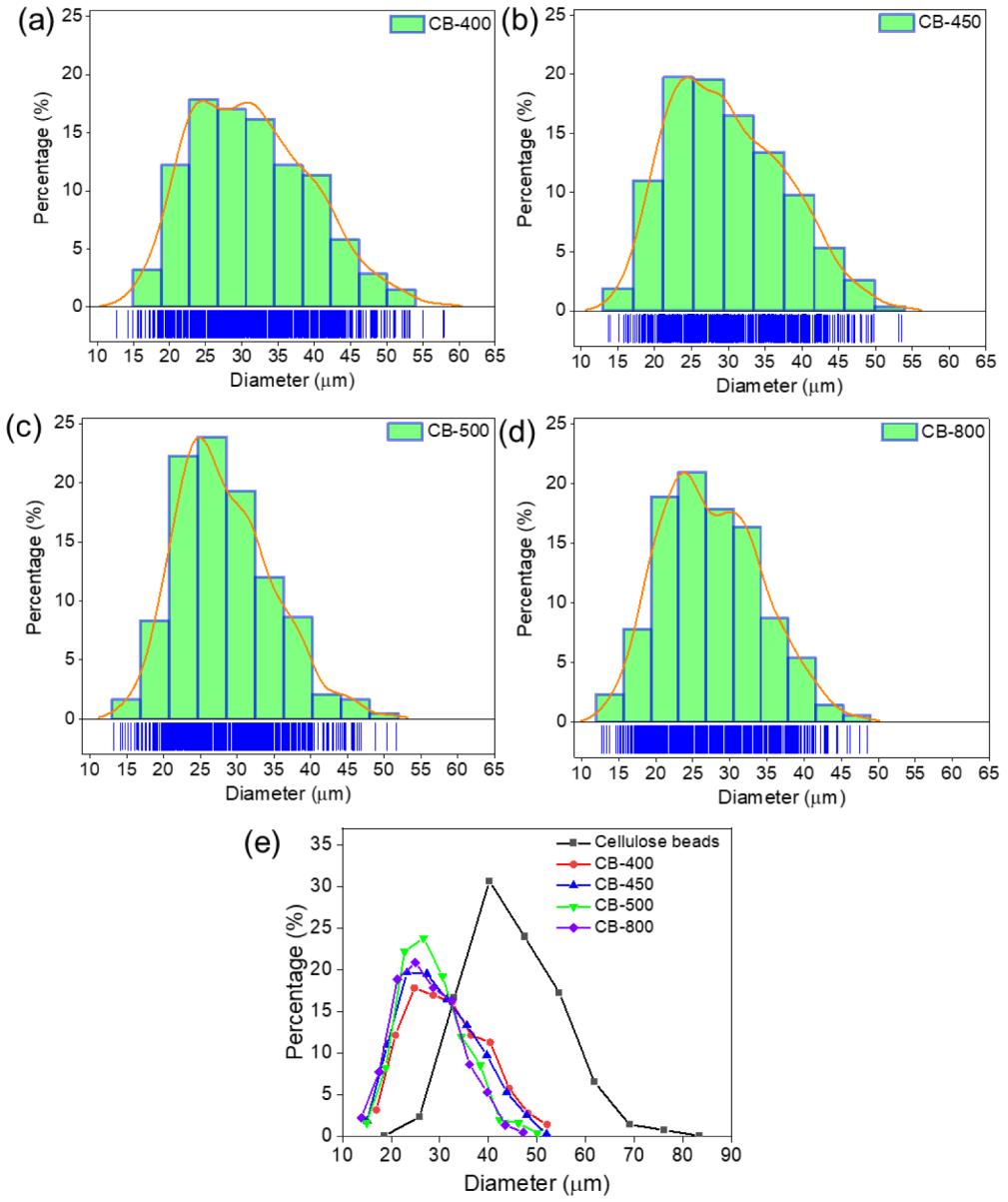

Figure 4. Particle size distribution of CB-400 (a), CB-450 (b), CB-500 (c), and CB-800 (d) and both cellulose and carbon beads (e).

Corporation. H_2SO_4 (95%−98%), HNO_3 (≥65%), $NaNO_3$ (≥99%), $BaCl_2$ (99.999%), $La(NO_3)_3{\cdot}6H_2O$ (99.99%), and $Bi(NO_3)_3{\cdot}5H_2O$ (98%) were obtained from Sigma-Aldrich, while NaCl (≥99.5%) and NaOH (≥99%) were acquired from Merck. HCl (37%) was supplied by Thermo Fisher Scientific. The chemicals and reagents were used as received without further purification. Ultrapure water with a resistivity of 18.2 MΩ·cm at 25 °C from a Milli-Q system was utilized to prepare the solutions.

2.2. Preparation of Spherical Carbon Beads. The commercially available spherical cellulose beads were subjected to drying using Rotavapor *R*-300 at 30 °C. Subsequently, the dried beads were carbonized in a Carbolite furnace under an argon atmosphere, maintaining a flow rate of 1000 mL min^{-1}. The cellulose beads were heated at a rate of 2 °C min^{-1} until the desired temperatures (e.g., 400, 450, 500, and 800 °C) were reached, followed by a holding period of 2 h. The samples were then cooled to room temperature at a rate of 2 °C min^{-1}. The obtained spherical carbon beads were then washed using Milli-Q water to remove any residual impurities from the quartz tube and crucible and subsequently dried in an oven at 70 °C. The washing step should be performed with care as insufficient washing might lead to aggregation of the beads during drying.

The obtained carbon bead (CB) was named CB-X (e.g., CB-400), where X °C represented the carbonization temperature used.

2.3. Preparation of Spherical Surface-Modified Carbon Beads. Initially, 0.7 g of carbon bead (CB-X) was added into a 100 mL round-bottom flask with a PTFE-coated magnet, and then, 70 mL of H_2SO_4 (95%−98%) was carefully added. Following that, the mixture was stirred at room temperature for 10 min and subsequently was heated at 150 °C for 3 h. The prepared samples were washed until no sulfuric acid was detectable using $BaCl_2$ as an indicator. The prepared sulfonated carbon beads were then dried in an oven at a temperature of 70 °C. Such carbon beads (SCBs) were denoted as SCB-X.

For the synthesis of oxidized carbon bead (OCB-400), HNO_3 was used as the reagent. First, 0.7 g of CB-400 was added to a

https://doi.org/10.1021/acsomega.4c05457
ACS Omega 2024, 9, 51009−51021

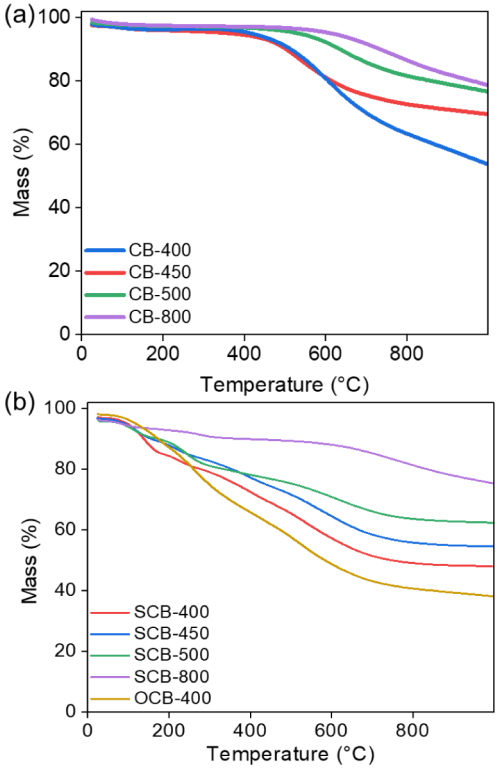

Figure 5. TGA curves of CB-400, CB-450, CB-500, and CB-800 (a) and SCB-400, SCB-450, SCB-500, SCB-800, and OCB-400 (b).

100 mL round-bottom flask with a PTFE-coated magnet, followed by the addition of 70 mL of HNO_3 (>65%). The mixture was then stirred at room temperature for 10 min and heated at 80 °C for 3 h. The prepared OCB-400 was washed thoroughly and then dried below 40 °C.

2.4. Batch Sorption Experiments. The batch sorption tests were performed according to the procedures outlined in the previous study.[17,18] In summary, a specific amount (10 or 30 mg) of the prepared sorbent was mixed with a 10 mL liquid phase containing either La^{3+}, Bi^{3+}, or a combination of both, along with varying concentrations of HNO_3, HCl, or $NaNO_3$. The mixture was stirred at a speed of 140 rpm for 24 h. To establish the initial metal concentrations, each liquid phase was compared with a blank solution without sorbents to provide a reference point for determining the initial metal concentration. The samples were then filtered using 0.45-μm syringe filters. The equilibrium concentrations of La^{3+} and Bi^{3+} were determined using ICP-MS (Thermo XSeries II quadrupole).

2.5. Characterization. The particle morphology, elemental composition, and distribution were examined by scanning electron microscopy (SEM, FEI Nova NanoSEM 450) and energy-dispersive X-ray spectrometry (EDS, Bruker Quantax200 EDS system). Particle size distributions were measured based on at least 3 SEM images, each representing 300 to 500 particles. The quantitative analysis of weight percentages for carbon, sulfur, and hydrogen was conducted using elemental analysis with Vario EL Cube (Elementar)/Vario Oxy Cube (Elementar). Multifunctional surface groups were identified using X-ray photoelectron spectroscopy (XPS, Kratos Axis Supra photoelectron spectrometer with a monochromated Al Kα ($h\nu$ = 1486.7 eV, 150 W) X-ray source and hemisphere analyzer). Thermogravimetric analysis (TGA, Netzsch STA 449 F3) was performed to investigate the thermal properties of the samples, under a flowing N_2 atmosphere (70 mL min^{-1}) at a heating rate of 10 °C min^{-1}. Prior to heating, the TGA equipment was flushed for 1 h with dry N_2 to remove residual oxygen in the furnace. During this time, also some adsorbed water might desorb from the samples, leading in some cases to an initial weight below 100%.

2.6. Equations. The separation performance of the samples was evaluated using the percentage removal (R) and distribution coefficient (K_d), which can be expressed as

$$R(\%) = \frac{C_o - C_e}{C_o} \times 100\% \quad (1)$$

$$K_d = \frac{(C_o - C_e)V}{C_e m} \quad (2)$$

where C_0 (μmol L^{-1}) and C_e (μmol L^{-1}) represent the initial concentration and equilibrium concentration, respectively, V (mL) is the suspension volume, and m (g) is the mass of sorbents. The error bars were calculated based on the measurement results and the equations used. In some cases, negative adsorption percentages are reported, which can be explained by the very low adsorption capacity of these materials under these experimental conditions and the accuracy of the ICP-MS method for the determination of C_0 and C_e.

3. RESULTS AND DISCUSSION

3.1. Characterization. SEM analysis was used to determine the morphology and structural characteristics of particles. Figures 2a–e illustrate the spherical shape of cellulose beads after the drying process. These particles appeared as distinct and individual spheres without any signs of clustering or aggregation. The surfaces of the particles were rough and textured, as observed in Figure 2d,e. In some particles, additional large open holes were observed, probably originating from the spheronization process (Figure 2a, b, and e). The particle sizes of the cellulose beads, as determined from the extracted SEM images,

Table 1. Elemental Compositions of Bulk Spherical Carbon Beads and Surface-Modified Carbon Beads

Samples	N [%]	C [%]	H [%]	S [%]	O [%]
CB-400	<0.1	79	4.0	<0.3	15.0
CB-450	0.1	84	3.5	<0.3	11.6
CB-500	0.5	86	3.0	<0.3	6.2
CB-800	0.5	93	1.2	<0.3	5.3
SCB-400	<0.1	58	3.1	2.9	37.5
SCB-450	<0.1	62	3.2	3.0	30
SCB-500	<0.1	68	2.9	5.0	25.6
SCB-800	0.3	92	1.0	0.9	7.2
OCB-400	4.1	54	2.9	<0.2	40

https://doi.org/10.1021/acsomega.4c05457
ACS Omega 2024, 9, 51009−51021

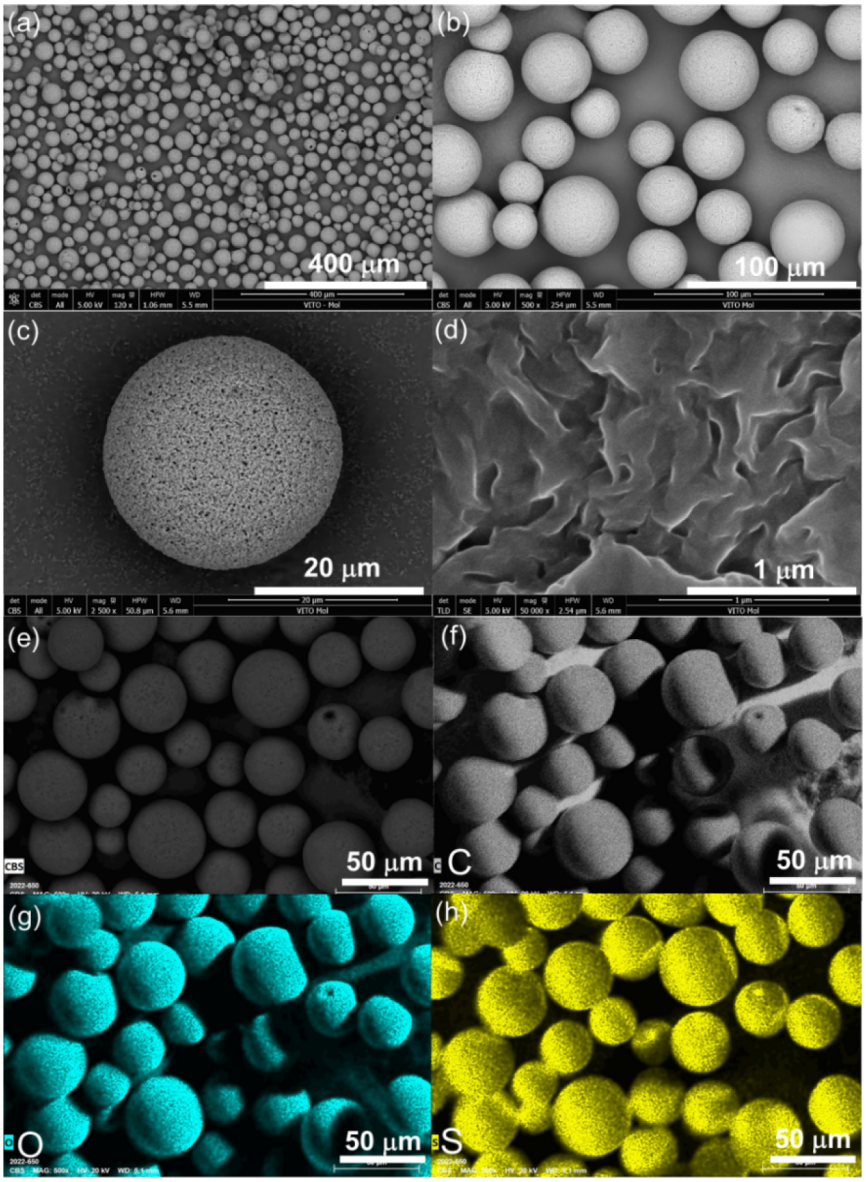

Figure 6. SEM images of SCB-400 (a−e) and element mapping images: C (f), O (g), and S (h).

ranged from 20 to 85 μm in diameter with a mean diameter of approximately 44 μm, as shown in Figure 2f.

The synthesis of carbon beads involved carbonization of dried cellulose beads at different temperatures. Based on previous research,[17] the following temperatures were selected: 400, 450, 500, and 800 °C. Figure 3 shows the morphology of the prepared carbon beads, CB-400, CB-450, CB-500, and CB-800. During carbonization, the carbon beads maintained their spherical shape and exhibited individual dispersion. Visible holes were observed on the surface of carbon beads due to the presence of such holes in the cellulose beads and the vaporization of volatile compounds. Figure 4 shows the particle size distribution of carbon beads. The mean diameters of CB-400, CB-450, CB-500, and CB-800 were approximately 31 (Figure 4a), 30 (Figure 4b), 28 (Figure 4c), and 27 (Figure 4d) μm, respectively. Despite variations in carbonization temperatures (as shown in TGA curves in Figure 5a), all carbon beads exhibited similar trends in particle size distribution. Notably, compared with the mean diameter of cellulose beads (approximately 44 μm), the particle size of carbon beads decreased to ∼29 μm (Figure 4e). This reduction in particle size could be attributed to the loss of volatile components, collapse of internal structures, or shrinkage during the carbonization process. To gain further insight into the internal structure of carbon beads, CB-450 was ground and then examined using SEM, as shown in Figure S1. The results revealed that the interior of the carbon beads appeared to be porous.

Table 1 presents the results of the elemental analysis for the carbonized beads. Carbon, hydrogen, and oxygen elements were found to be the primary elements in the carbon beads. As the carbonization temperature increased from 400 to 800 °C, the bulk carbon content in carbon beads increased from 79 wt % to 93 wt %. This increase in carbon content was assigned to a loss of the hetero elements, as the bulk hydrogen and oxygen contents decreased from 4 wt % to 1.2 wt % and from 15 wt % to 5.3 wt %, respectively, suggesting the further decomposition of precursor structures. When carbonized at 800 °C, the bead consisted of 93 wt % carbon. Notably, no sulfur contents higher than the detection limit could be measured in any of the carbon beads.

https://doi.org/10.1021/acsomega.4c05457
ACS Omega 2024, 9, 51009−51021

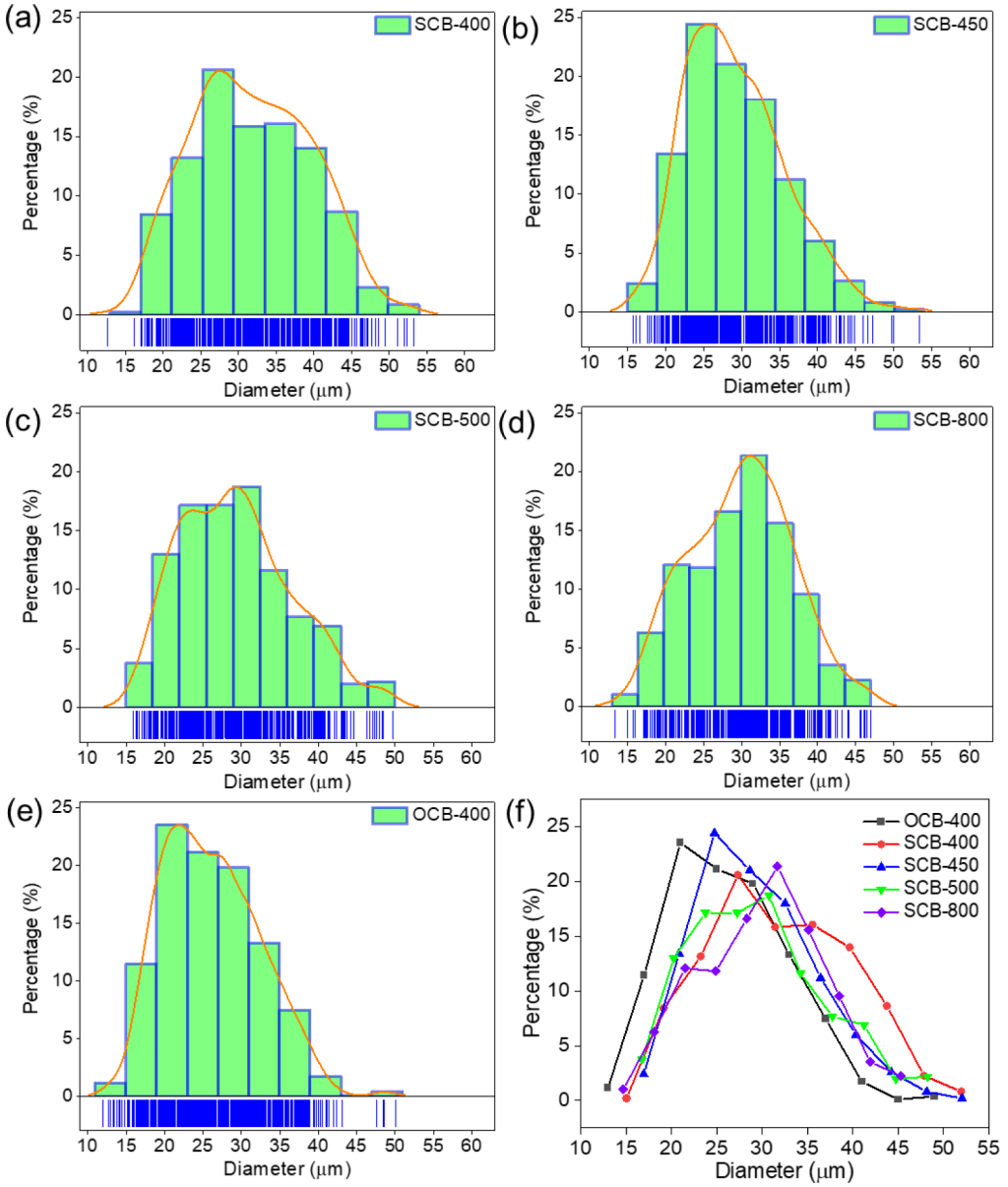

Figure 7. Particle size distribution of SCB-400 (a), SCB-450 (b), SCB-500 (c), SCB-800 (d), OCB-400 (e), and all spherical surface-modified carbon beads (f).

These carbon beads were surface-modified by subjecting them to the sulfonation process using concentrated sulfuric acid as the reagent. SEM images and particle size distributions are shown in Figures 6, S2−S4, and 7, respectively. The sulfonated carbon beads maintained their spherical shape without any signs of particle disintegration. Moreover, the individual particle dispersion was observed without aggregation. Like the crushed CB-450, SEM images of ground SCB-450 (Figure S5) indicated that the majority of particles exhibited a solid interior with observable inner-bead holes.

The mean diameters of SCB-400, SCB-450, SCB-500, and SCB-800 were determined to be 32 (Figure 7a), 29 (Figure 7b), 29 (Figure 7c), and 30 (Figure 7d) μm, respectively. These values indicated that the particle sizes of the carbon beads did not undergo significant changes before and after the sulfonation process, suggesting that the carbon structures exhibited high acid stability. Compared to pristine carbon materials (Figure 5a), the TGA curves also revealed high decomposition for SCB-400, SCB-450, SCB-500, and SCB-800 (Figure 5b), indicating the presence of grafted functional groups on the surface of these spherical pristine carbon materials. Furthermore, to prevent degradation of such functional groups, it is advisible to utilize these surface-modified carbon materials below 150 °C. The changes in elemental composition after sulfonation were measured by elemental analysis (Table 1). A first observation was a large increase of oxygen and to a lesser extent sulfur for all samples after sulfonation, regardless of the carbonization temperature. Sulfur levels increased from 2.9 wt % to 5 wt %, as carbonization temperature increased from 400 to 500 °C. The introduction of oxygen- and sulfur-containing groups seemed to be less effective for the carbon beads carbonized at 800 °C, as elemental composition was unaltered after sulfonation. A similar observation was made in our previous paper on the pyrolysis of the methyl cellulose.[17]

EDS analysis results of the carbon surface after sulfonation demonstrated the uniform distribution of the elements (Figures

https://doi.org/10.1021/acsomega.4c05457
ACS Omega 2024, 9, 51009−51021

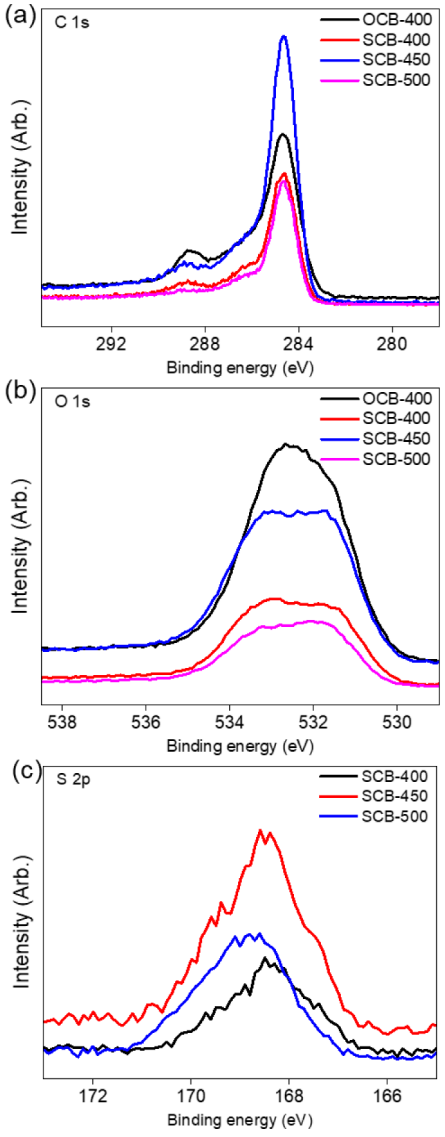

Figure 8. High-resolution XPS spectra of C 1s (a), O 1s (b), and S 2p (c) of spherical surface-modified carbon beads.

S6, 6 f–h, S2 f–h, and S3 f–h). The detailed information on EDS analysis can be seen in Supporting Information. However, it is also important to consider other influencing variables, such as differences in carbonization conditions and sulfonation times.[17,18]

The nature and amount of the sulfur- and oxygen-containing groups were determined from XPS analysis. The peak with high binding energy in the S 2p region (166–171 eV) indicated the presence of oxidized sulfur-containing groups (Figures 8, S8–S12, and Table S3), analogous to the spectra of the pyrolyzed and sulfonated methyl cellulose in our previous work.[17] The content of surface sulfur followed the same order as that measured by the elemental analysis (Table S3): SCB-400 (0.9 at. %) < SCB-450 (1.1 at. %) < SCB-500 (1.7 at. %).

The C 1s XPS analysis showed that a decrease in surface O–C═O content (Table S1) was observed with increasing carbonization temperature (SCB-400 (4.6 at. %) > SCB-450 (3.5 at. %) > SCB-500 (2.7 at. %)). Carbon materials subjected to lower carbonization temperatures could be grafted with more oxygen-containing groups, possibly due to the presence of more defect sites in the carbon structures. The identified oxygen-containing groups (Tables S1–S3) could be attributed to carboxylic, phenyl, and carbonyl groups. These findings support the expectation that functional groups can be grafted onto carbon structures at relatively low carbonization temperatures. Additionally, it suggests that carbon materials with higher carbonization temperatures are suitable as supports for extraction chromatography, minimizing the impact of the introduction of oxygen-containing groups on carbon structures due to irradiation.[24]

In contrast, the synthesized oxidized carbon beads did not contain sulfur and served as a reference to assess active sorption sites (Figure S6d). The morphology of OCB-400 closely resembled that of SCB-400, as shown in Figure S7. However, OCB-400 exhibited a slightly reduced mean diameter of approximately 26 μm (Figure 7e) compared to that of SCB-400, which had a mean diameter of 32 μm. This reduction in the size might be attributed to the harsh conditions in the hot HNO_3 solutions. The particle size distribution curve of OCB-400 shifted slightly toward smaller diameters (Figure 7f).

3.2. Separation Performance. Batch sorption experiments were conducted to evaluate the La^{3+} and Bi^{3+} sorption onto the prepared sorbents. Based on our previous research, specific factors such as HNO_3 and $NaNO_3$ concentrations were carefully controlled to selectively adsorb Bi^{3+} while minimizing the sorption of La^{3+} (as a surrogate of Ac^{3+}).[17,18] Furthermore, HCl was identified as a suitable eluent for effectively eluting Bi^{3+} from sorbents.[13,17,18,32,33]

The sorption percentages of SCB-500 toward Bi^{3+} were determined to be 6% ± 0.8% and 16% ± 3.3%, at solid-to-liquid ratios of 1 g L^{-1} and 5 g L^{-1}, with a pH of 2, respectively. SCB-500 was not further investigated in subsequent experiments because of its relatively low Bi^{3+} sorption capacity. Therefore, SCB-400, SCB-450, and OCB-400 were selected as the primary samples for further investigation.

3.2.1. Effect of HNO_3 Concentration. The concentration of acid plays a critical role in determining the sorption capacity of materials for metal ions.[18] This is attributed to the influence of surface functional groups and the presence of metal species in the aqueous environment. Under acidic conditions with a pH below 2, both La^{3+} and Bi^{3+} exist primarily as cations.[17] Figures 9a–c illustrate that the sorption performance of SCB-400, SCB-450, and OCB-400 decreased as the concentration of HNO_3 increased, due to the competition effect of H^+. In a 0.1 M HNO_3 solution, the Bi^{3+} sorption capacity followed the order SCB-400 > OCB-400 > SCB-450, indicating a higher density of the sorption active sites on the surface of SCB-400 and OCB-400. The observed decrease in sorption capacity as the acid concentration increased was much more pronounced for La^{3+} compared to Bi^{3+}.[34,35] The stronger affinity for Bi^{3+} could be assigned to the Bi speciation in which the presence of hydrolyzed species exhibited a stronger affinity for oxygen donors. This phenomenon also aligns with an increasing trend in the $\log_{10} K$ values for the first hydrolysis step for Bi^{3+} (−1.1) and La^{3+} (−8.4).[18] Consequently, it was suggested that SCB-400, SCB-450, and OCB-400 could selectively adsorb Bi^{3+} in relatively highly acidic solutions (e.g., 0.3–1 mol L^{-1}). Furthermore, compared to SCB-400 and OCB-400, the sorption capacity of SCB-450 for Bi^{3+} was susceptible to changes in the H^+ concentration. Therefore, precise control of the acid concentration is expected to provide a means for selective Bi^{3+} sorption onto the inverse columns.

3.2.2. Effect of $NaNO_3$ Concentration. The concentration of the salt is another crucial factor in the separation of Bi^{3+} from

https://doi.org/10.1021/acsomega.4c05457
ACS Omega 2024, 9, 51009−51021

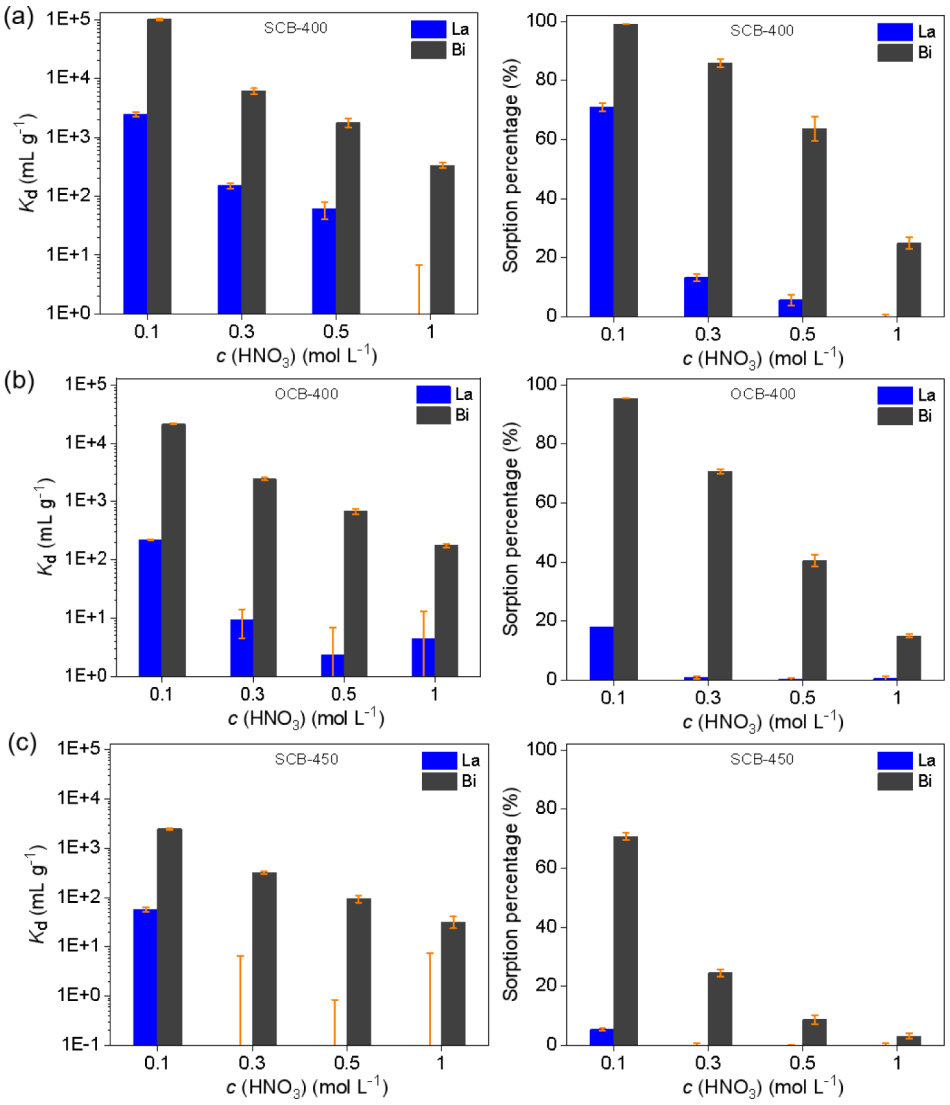

Figure 9. Effect of HNO_3 concentration on the sorption performance of SCB-400 (a), OCB-400 (b), and SCB-450 (c) for La^{3+}/Bi^{3+} (C_o (La^{3+}) = 10 μmol L^{-1}, C_o (Bi^{3+}) = 10 μmol L^{-1}, S: L = 1 g L^{-1}, t = 24 h, binary system).

La^{3+} for surface-modified carbon materials. One of the effects of increasing the salt concentration is its impact on the electrical double-layer structure on the surface of sorbents, resulting in a thinner overall double layer and more effective screening of the surface by the salt ions.[36] Figures 10−12 present the sorption performance of SCB-400, OCB-400, and SCB-450 at different $NaNO_3$ concentrations, at pH = 1 and pH = 0.5, respectively.

Figure 10 shows the significant decrease in sorption of La^{3+} onto SCB-400 as the $NaNO_3$ concentration increased from 0.1 to 2 mol L^{-1} at pH = 1. However, reducing the sorption of La^{3+} on SCB-400 to near zero (the mean value) becomes challenging, even when 2 mol L^{-1} $NaNO_3$ was used (Figure 10a). Reducing the pH to 0.5 led to the same trends in sorption for both La^{3+} and Bi^{3+} (Figure 10b) but showed that when the $NaNO_3$ concentration exceeded 0.5 mol L^{-},[1] the adsorbed fraction of La^{3+} was close to zero. In contrast, the sorption percentage for Bi^{3+} remained above 50%. These findings indicate that the selective sorption of Bi^{3+} onto SCB-400 is expected to be achieved by adjusting both acid and salt concentrations.

Similar observations could be made for the Bi^{3+} and La^{3+} sorption capacity of OCB-400 (Figure 11), but overall values were lower than those of SCB-400, with La^{3+} sorption already at zero at pH = 1 and a $NaNO_3$ concentration of 0.5 mol L^{-1} (Figure 11a). Under these conditions, the Bi^{3+} sorption capacity remained high. These results indicated that sulfonation and oxidation treatments had a strong influence on La^{3+} sorption caused by a change in functional groups and carbon structures, where significant modifications in carbon structures and functional groups with oxidation treatment were observed, particularly with nitric acid.[18] As the pH decreased further to 0.5 (Figure 11b), the sorption performance of OCB-400 for La^{3+} almost disappeared in the presence of 0.1−2 M $NaNO_3$. These findings suggested a more selective sorption of Bi^{3+} onto OCB-400 compared to SCB-400. However, due to insufficient data, this study cannot conclusively determine whether oxidation treatment is superior to sulfonation treatment. Future experiments should focus on evaluating the sorption performance of oxidized carbon materials for La^{3+} and Bi^{3+}. Nonetheless, based on sorption mechanisms, using sulfonated carbon materials in an inverse generator might be analogous to using spherical oxidized carbon beads in the same setup, although further investigation is needed to validate this hypothesis.

The lowest sorption capacities for both Bi^{3+} and La^{3+} were observed for SCB-450 (Figure 12). As already discussed, the

https://doi.org/10.1021/acsomega.4c05457
ACS Omega 2024, 9, 51009−51021

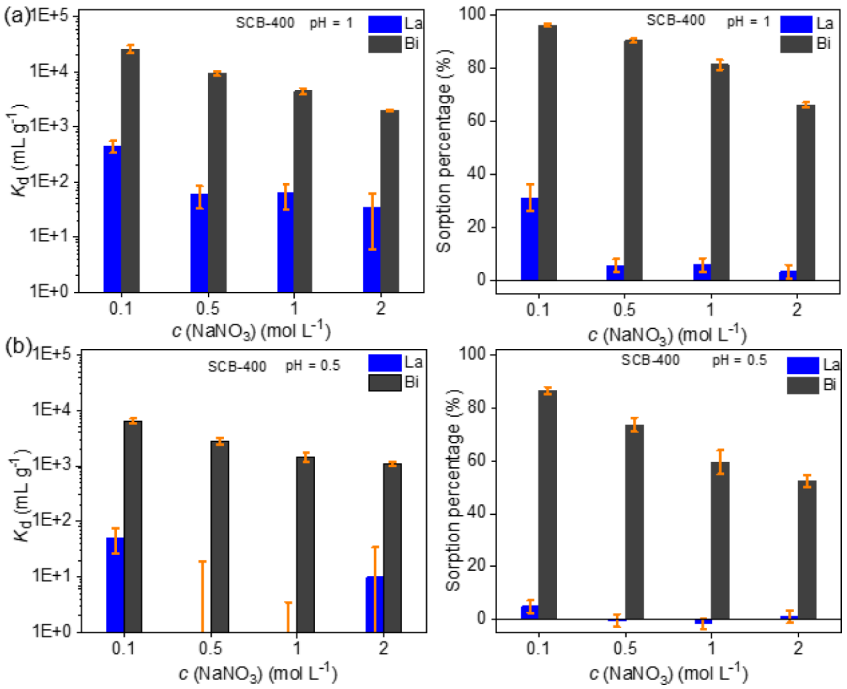

Figure 10. Effect of $NaNO_3$ concentration for La^{3+} and Bi^{3+} sorption onto SCB-400 at pH = 1 (a) and pH = 0.5 (b) (C_o (La^{3+}) = 10 μmol L^{-1}, C_o (Bi^{3+}) = 10 μmol L^{-1}, S: L = 1 g L^{-1}, t = 24 h, binary system).

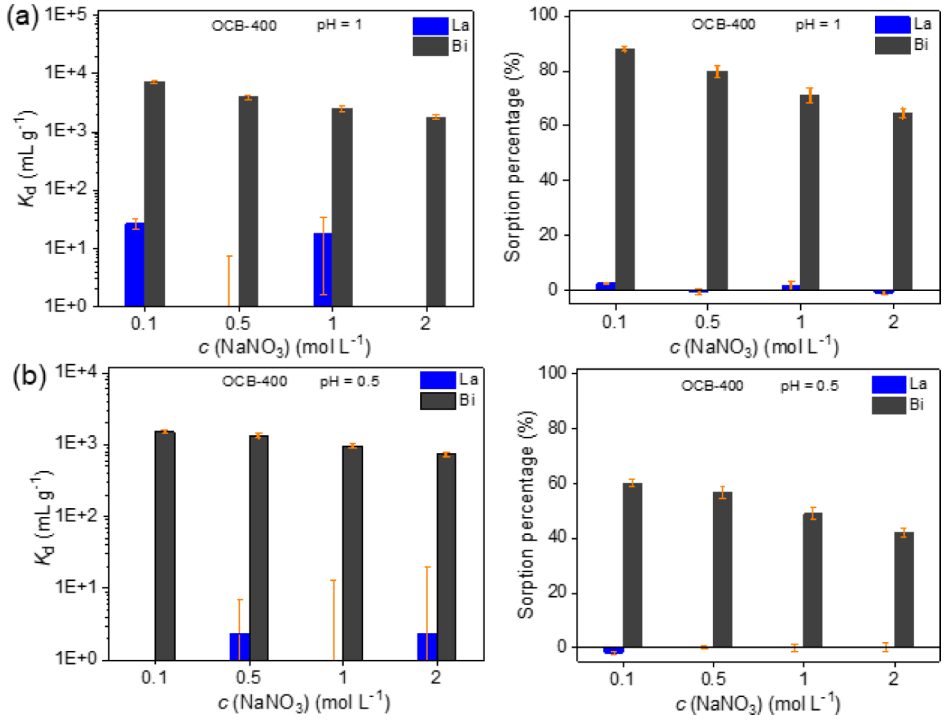

Figure 11. Effect of $NaNO_3$ concentration for La^{3+} and Bi^{3+} sorption onto OCB-400 at pH = 1 (a) and pH = 0.5 (b) (C_o (La^{3+}) = 10 μmol L^{-1}, C_o (Bi^{3+}) = 10 μmol L^{-1}, S: L = 1 g L^{-1}, t = 24 h, binary system).

differences in carbon structures affect the quantity and properties of the surface functional groups. The sorption capacity of SCB-450 for La^{3+} (Figure 12a) was close to zero at a $NaNO_3$ concentration of 0.1 mol L^{-1}. With increasing $NaNO_3$ concentration, the sorption capacity of SCB-450 for La^{3+} remained near zero, but the sorption capacity for Bi^{3+} also decreased. At a $NaNO_3$ concentration of approximately 0.5 mol L^{-1}, the sorption percentage of SCB-450 for Bi^{3+} was approximately 35%. Furthermore, the sorption percentage for Bi^{3+} remained at 20%, even at a $NaNO_3$ concentration of 2 mol L^{-1}. Similar trends were observed at pH = 0.5, as shown in Figure 12b. Compared with SCB-400, it is expected that the utilization of acid and salt concentrations can be reduced.

3.2.3. Effect of HCl Concentration. Given the influence of acid and salt concentrations, Bi^{3+} is expected to be selectively adsorbed onto the spherical surface-modified carbon beads, in

https://doi.org/10.1021/acsomega.4c05457
ACS Omega 2024, 9, 51009−51021

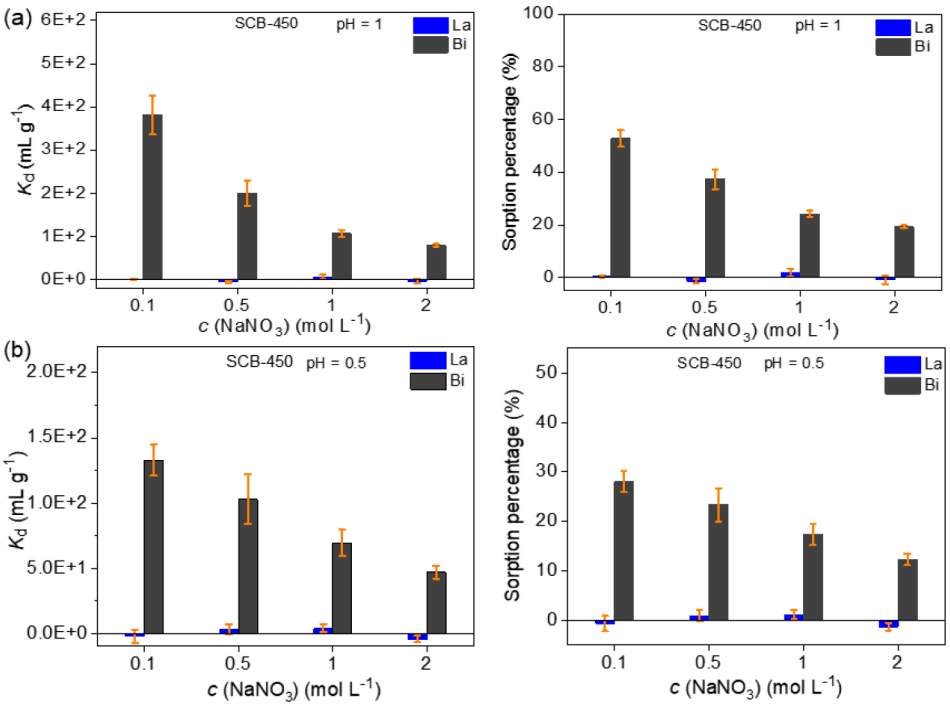

Figure 12. Effect of $NaNO_3$ concentration for La^{3+} and Bi^{3+} sorption onto SCB-450 at pH = 1 (a) and pH = 0.5 (b) (C_o (La^{3+}) = 10 μmol L^{-1}, C_o (Bi^{3+}) = 10 μmol L^{-1}, S: L = 3 g L^{-1}, t = 24 h, binary system).

accordance with our previous studies.[17,18] The next step involves examining the desorption performance of Bi^{3+} from these beads. Typically, HCl is used as an eluent to remove Bi^{3+} from the inverse generators. Unlike NaI eluent, using HCl does not alter the color of the ^{213}Bi eluate, eliminating the need for decoloring agents.[14] The low sorption capacity of Bi^{3+} in HCl solutions suggests that a high Bi^{3+} yield could be obtained from the column by using low HCl concentrations and volumes.

Figure 13 depicts the sorption percentages of SCB-400, OCB-400, and SCB-450 as a function of the HCl concentrations. For all carbon materials, the sorption percentage for La^{3+} and Bi^{3+} decreased as the HCl concentration increased, but the mechanism behind the decrease was different. The sorption percentage for La^{3+} on surface-modified carbon beads decreased due to the competitive sorption of H^+ and the increased ionic strength. The sorption percentage of Bi^{3+} decreased mainly due to the formation of Bi−Cl complexes and the competitive sorption of H^+.[37] OCB-400 and SCB-450 exhibited a sorption capacity for Bi^{3+} that approached zero starting from 0.3 mol L^{-1} HCl compared to SCB-400. This suggested that Bi^{3+} could be easily desorbed from the surface of OCB-400 and SCB-450 using relatively low HCl concentrations compared to SCB-400.

4. CONCLUSION AND OUTLOOK

In conclusion, the synthesis of spherical surface-modified carbon beads was successfully achieved through the pyrolysis of spherical cellulose beads as a carbon precursor, followed by sulfonation and oxidation treatments. The prepared carbon beads exhibited reduced particle sizes compared with the cellulose beads. Various functional groups were grafted onto the surfaces of the spherical carbon structures and enhanced if a relatively low carbonization temperature was used. All surface-modified carbon materials had a higher affinity for Bi^{3+} than for La^{3+}. The sorption performance could be tailored by adjusting the sorption conditions, including the acid and salt concentrations. These preliminary findings indicate that SCB-400, OCB-400, and SCB-500 can potentially be used as inverse generators for the separation of ^{225}Ac and ^{213}Bi.

However, before the real potential of these materials can be assessed for their application in a ^{225}Ac/^{213}Bi generator, more research is required, both on the materials and on the separation process itself. One aspect that needs improvement is the synthesis protocol to obtain the spherical beads. Using cellulose as a precursor will only yield a small fraction of carbonized beads, typically less than ∼20%, due to the vaporization of volatile compounds during carbonization. To overcome this limitation, alternative approaches, such as selecting a carbon precursor of predominantly aromatic ring structure or the coating of preformed spherical inorganic materials with cellulose, could be explored. Additionally, further research should focus on examining the impact of particle size in column chromatography by synthesizing carbon beads with varying sizes within the range of 20−300 μm. Although this presents a significant challenge, it holds significant potential for advancing further in this research field.

■ ASSOCIATED CONTENT

Supporting Information

The Supporting Information is available free of charge at https://pubs.acs.org/doi/10.1021/acsomega.4c05457.

SEM images (Figures S1−S5 and S7), EDS spectra (Figure S6) and XPS spectra (Figures S8−S12), and fitting data (Tables S1−S3) (PDF)

■ AUTHOR INFORMATION

Corresponding Author

Thomas Cardinaels − *Belgian Nuclear Research Centre (SCK CEN), Institute for Nuclear Materials Science, Mol B-2400, Belgium; KU Leuven, Department of Chemistry, Leuven B-*

https://doi.org/10.1021/acsomega.4c05457
ACS Omega 2024, 9, 51009−51021

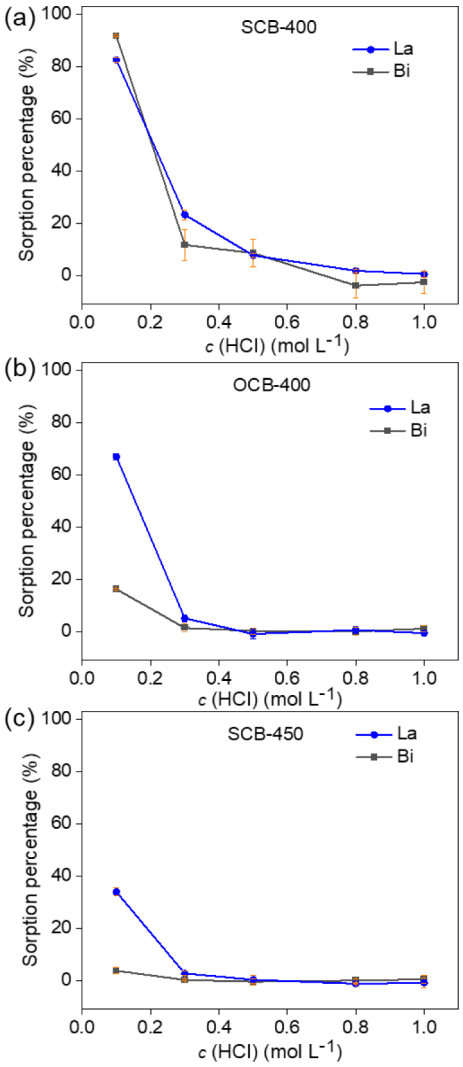

Figure 13. Effect of HCl concentration for the sorption performance of SCB-400 (a), OCB-400 (b), and SCB-450 (c) for La^{3+}/Bi^{3+} (C_o (La^{3+}) = 10 μmol L^{-1}, C_o (Bi^{3+}) = 10 μmol L^{-1}, S: L = 1 g L^{-1}, t = 24 h, binary system).

3001, Belgium; orcid.org/0000-0002-2695-1002; Email: thomas.cardinaels@kuleuven.be

Authors

Hongshan Zhu − *Belgian Nuclear Research Centre (SCK CEN), Institute for Nuclear Materials Science, Mol B-2400, Belgium; KU Leuven, Department of Chemistry, Leuven B-3001, Belgium; Flemish Institute for Technological Research (VITO NV), Sustainable Materials Management, Mol B-2400, Belgium;* Present Address: CAS Key Laboratory of Separation Science for Analytical Chemistry, Dalian Institute of Chemical Physics, Chinese Academy of Sciences, Dalian, 116023 P. R. China

Stephan Heinitz − *Belgian Nuclear Research Centre (SCK CEN), Institute for Nuclear Materials Science, Mol B-2400, Belgium*

Koen Binnemans − *KU Leuven, Department of Chemistry, Leuven B-3001, Belgium;* orcid.org/0000-0003-4768-3606

Steven Mullens − *Flemish Institute for Technological Research (VITO NV), Sustainable Materials Management, Mol B-2400, Belgium*

Complete contact information is available at: https://pubs.acs.org/10.1021/acsomega.4c05457

Author Contributions

H.Z.: conceptualization, data curation, formal analysis, investigation, methodology, validation, visualization, writing−original draft. S.H.: conceptualization, formal analysis, investigation, methodology, visualization, writing−review and editing, funding acquisition. K.B.: conceptualization, supervision, formal analysis, investigation, methodology, visualization, writing−review and editing, funding acquisition. S.M.: conceptualization, formal analysis, investigation, methodology, visualization, writing−review and editing, funding acquisition. T.C.: conceptualization, supervision, formal analysis, investigation, methodology, visualization, writing−review and editing, funding acquisition.

Notes

The authors declare no competing financial interest.

■ ACKNOWLEDGMENTS

The SCK CEN Academy and VITO are acknowledged for funding. Furthermore, the authors would like to acknowledge the technical assistance of Prisca Verheyen (ICP-MS), Samuel Eyley and Wim Thielemans (XPS), and Kemps Raymond (SEM).

■ REFERENCES

(1) Sgouros, G.; Bodei, L.; McDevitt, M. R.; Nedrow, J. R. Radiopharmaceutical therapy in cancer: Clinical advances and challenges. *Nat. Rev. Drug Discovery* **2020**, *19* (9), 589−608.

(2) St. James, S.; Bednarz, B.; Benedict, S.; Buchsbaum, J. C.; Dewaraja, Y.; Frey, E.; Hobbs, R.; Grudzinski, J.; Roncali, E.; Sgouros, G.; et al. Current Status of Radiopharmaceutical Therapy. *Int. J. Radiat. Oncol. Biol. Phys.* **2021**, *109* (4), 891−901.

(3) Ferrier, M. G.; Radchenko, V.; Wilbur, D. S. Radiochemical aspects of alpha emitting radionuclides for medical application. *Radiochim. Acta.* **2019**, *107* (9−11), 1065−1085.

(4) Eychenne, R.; Chérel, M.; Haddad, F.; Guérard, F.; Gestin, J.-F. Overview of the Most Promising Radionuclides for Targeted Alpha Therapy: The "Hopeful Eight. *Pharmaceutics* **2021**, *13* (6), 906.

(5) Ahenkorah, S.; Cassells, I.; Deroose, C. M.; Cardinaels, T.; Burgoyne, A. R.; Bormans, G.; Ooms, M.; Cleeren, F. Bismuth-213 for Targeted Radionuclide Therapy: From Atom to Bedside. *Pharmaceutics* **2021**, *13* (5), 599.

(6) Horváth, D.; Travagin, F.; Guidolin, N.; Buonsanti, F.; Tircsó, G.; Tóth, I.; Bruchertseifer, F.; Morgenstern, A.; Notni, J.; Giovenzana, G. B.; Baranyai, Z. Towards ^{213}Bi alpha-therapeutics and beyond: Unravelling the foundations of efficient Bi^{III} complexation by DOTP. *Inorg. Chem. Front.* **2021**, *8* (16), 3893−3904.

(7) Zhu, H.; Heinitz, S.; Binnemans, K.; Mullens, S.; Cardinaels, T. ^{225}Ac/^{213}Bi radionuclide generators for the separation of ^{213}Bi towards clinical demands. *Inorg. Chem. Front.* **2024**, *11*, 4499−4527.

(8) Vasiliev, A. N.; Zobnin, V. A.; Pavlov, Y. S.; Chudakov, V. M. Radiation Stability of Sorbents in Medical ^{225}Ac/^{213}Bi Generators. *Solvent Extr. Ion Exch.* **2021**, *39* (4), 353−372.

(9) Ermolaev, S.; Skasyrskaya, A.; Vasiliev, A. A Radionuclide Generator of High-Purity Bi-213 for Instant Labeling. *Pharmaceutics* **2021**, *13* (6), 914.

(10) Morgenstern, A.; Bruchertseifer, F.; Apostolidis, C. Bismuth-213 and actinium-225−generator performance and evolving therapeutic applications of two generator-derived alpha-emitting radioisotopes. *Curr. Radiopharm.* **2012**, *5* (3), 221−227.

(11) McAlister, D. R.; Philip Horwitz, E. Automated two column generator systems for medical radionuclides. *Appl. Radiat. Isot.* **2009**, *67* (11), 1985−1991.

(12) Bray, L. A.; Tingey, J. M.; DesChane, J. R.; Egorov, O. B.; Tenforde, T. S.; Wilbur, D. S.; Hamlin, D. K.; Pathare, P. M.

Development of a Unique Bismuth (Bi-213) Automated Generator for Use in Cancer Therapy. *Ind. Eng. Chem. Res.* **2000**, *39* (9), 3189−3194.
(13) Vasiliev, A. N.; Ermolaev, S. V.; Lapshina, E. V.; Zhuikov, B. L.; Betenekov, N. D. $^{225}Ac/^{213}Bi$ generator based on inorganic sorbents. *Radiochim. Acta.* **2019**, *107* (12), 1203−1211.
(14) McDevitt, M. R.; Finn, R. D.; Sgouros, G.; Ma, D.; Scheinberg, D. A. An $^{225}Ac/^{213}Bi$ generator system for therapeutic clinical applications: Construction and operation. *Appl. Radiat. Isot.* **1999**, *50* (5), 895−904.
(15) Ondrák, L.; Ondrák Fialová, K.; Sakmár, M.; Vlk, M.; Štamberg, K.; Drtinová, B.; Šlouf, M.; Bruchertseifer, F.; Morgenstern, A.; Kozempel, J. Preparation and characterization of α-zirconium phosphate as a perspective material for separation of ^{225}Ac and ^{213}Bi. *J. Radioanal. Nucl. Chem.* **2023**, *332* (5), 1475−1481.
(16) Kazanjian, A. R.; Killion, M. E. *Radiation effects on Amberlite IRA-938 and bio-rad AG MP-50 ion exchange resins*; Rockwell International Corp., Rocky Flats Plant: Golden, United States, 1982, pp. RFP−3167. .
(17) Zhu, H.; Heinitz, S.; Eyley, S.; Thielemans, W.; Binnemans, K.; Mullens, S.; Cardinaels, T. Selective separation of Bi^{3+} from La^{3+}/Ac^{3+} by sorption on sulfonated carbon materials for use in an inverse $^{225}Ac/^{213}Bi$ radionuclide generator: Batch and column tests. *Chem. Eng. J.* **2023**, *468*, 143416.
(18) Zhu, H.; Heinitz, S.; Eyley, S.; Thielemans, W.; Binnemans, K.; Mullens, S.; Cardinaels, T. Sorption and desorption performance of La^{3+}/Bi^{3+} by surface-modified activated carbon for potential application in medical $^{225}Ac/^{213}Bi$ generators. *Chem. Eng. J.* **2023**, *464*, 142456.
(19) Wu, C.; Brechbiel, M. W.; Gansow, O. A. An Improved Generator for the Production of ^{213}Bi from ^{225}Ac. *Radiochim. Acta.* **1997**, *79* (2), 141−144.
(20) Dash, A.; Chakravarty, R. Pivotal role of separation chemistry in the development of radionuclide generators to meet clinical demands. *RSC Adv.* **2014**, *4* (81), 42779−42803.
(21) Dash, A.; Knapp, J. F. F., Jr; Pillai, M. R. A. Industrial radionuclide generators: A potential step towards accelerating radiotracer investigations in industry. *RSC Adv.* **2013**, *3* (35), 14890−14909.
(22) Betenekov, N. D.; Denisov, E. I.; Vasiliev, A. N.; Ermolaev, S. V.; Zhuikov, B. L. Prospects for the Development of an $^{225}Ac/^{213}Bi$ Generator Using Inorganic Hydroxide Sorbents. *Radiochemistry* **2019**, *61* (2), 211−219.
(23) Zhuikov, B. L.; Ermolaev, S. V. Radioisotope research and development at the Linear Accelerator of the Institute for Nuclear Research of RAS. *Physics-Uspekhi.* **2021**, *64* (12), 1311.
(24) Zhu, H.; Heinitz, S.; Eyley, S.; Thielemans, W.; Derveaux, E.; Adriaensens, P.; Binnemans, K.; Mullens, S.; Cardinaels, T. Gamma radiation effects on AG MP-50 cation exchange resin and sulfonated activated carbon for bismuth-213 separation. *RSC Adv.* **2023**, *13* (44), 30990−31001.
(25) Unger, K. K.; Skudas, R.; Schulte, M. M. Particle packed columns and monolithic columns in high-performance liquid chromatography-comparison and critical appraisal. *J. Chromatogr. A* **2008**, *1184* (1), 393−415.
(26) Dolamore, F.; Fee, C.; Dimartino, S. Modelling ordered packed beds of spheres: The importance of bed orientation and the influence of tortuosity on dispersion. *J. Chromatogr. A* **2018**, *1532*, 150−160.
(27) Gericke, M.; Trygg, J.; Fardim, P. Functional Cellulose Beads: Preparation, Characterization, and Applications. *Chem. Rev.* **2013**, *113* (7), 4812−4836.
(28) Ouzzine, M.; Romero-Anaya, A. J.; Lillo-Ródenas, M. A.; Linares-Solano, A. Spherical activated carbons for the adsorption of a real multicomponent VOC mixture. *Carbon* **2019**, *148*, 214−223.
(29) Long, L. Y.; Weng, Y. X.; Wang, Y. Z. Cellulose Aerogels: Synthesis, Applications, and Prospects. *Polymers* **2018**, *10* (6), 623.
(30) Tsubota, T.; Nagata, D.; Murakami, N.; Ohno, T. Spherical activated carbon derived from spherical cellulose and its performance as EDLC electrode. *J. Appl. Polym. Sci.* **2014**, *131* (20), 40950.
(31) Nagaoka, S.; Ihara, H.; Honbo, J.; Hirayama, C.; Kurisaki, H.; Ikegami, S. Spherical Carbon Packings Prepared from Spherical Cellulose Particles for High-Performance Liquid Chromatography. *Anal. Sci.* **1994**, *10* (4), 543−551.
(32) Boldyrev, P. P.; Deev, S. M.; Golovachenko, V. A.; Zagryadskii, V. A.; Zakharov, A. S.; Nikolaev, V. I.; Nurtdinov, R. F.; Proshin, M. A.; Chuvilin, D. Y.; Yashin, Y. A. Determination of the labeling yield and stability of the complexes Bi-BSA-DOTA and Bi-BSA-DTPA. *Radiochemistry* **2014**, *56* (2), 194−199.
(33) Sinenko, I. L.; Kalmykova, T. P.; Likhosherstova, D. V.; Egorova, B. V.; Zubenko, A. D.; Vasiliev, A. N.; Ermolaev, S. V.; Lapshina, E. V.; Ostapenko, V. S.; Fedorova, O. A.; Kalmykov, S. N. ^{213}Bi production and complexation with new picolinate containing ligands. *J. Radioanal. Nucl. Chem.* **2019**, *321* (2), 531−540.
(34) Hassfjell, S.; Brechbiel, M. W. The Development of the α-Particle Emitting Radionuclides ^{212}Bi and ^{213}Bi, and Their Decay Chain Related Radionuclides, for Therapeutic Applications. *Chem. Rev.* **2001**, *101* (7), 2019−2036.
(35) Kleja, D. B.; Gustafsson, J. P.; Kessler, V.; Persson, I. B. (. Bismuth(III) Forms Exceptionally Strong Complexes with Natural Organic Matter. *Environ. Sci. Technol.* **2022**, *56* (5), 3076−3084.
(36) Zhang, Y.; Zhu, C.; Liu, F.; Yuan, Y.; Wu, H.; Li, A. Effects of ionic strength on removal of toxic pollutants from aqueous media with multifarious adsorbents: A review. *Sci. Total Environ.* **2019**, *646*, 265−279.
(37) Jurinak, J. J. The hydrolysis of cations.Soil Sci. *Soc. Am. J.* **1976**, *40*, 3, .

https://doi.org/10.1021/acsomega.4c05457
ACS Omega 2024, 9, 51009−51021